Available online at www.sciencedirect.com

SciVerse ScienceDirect

Ceramics International 39 (2013) 4619–4625

CERAMICS INTERNATIONAL

www.elsevier.com/locate/ceramint

Short communication

Microemulsion-mediated synthesis and characterization of monodispersed nickel molybdate nanocrystals

M. Masteri-Farahani[a,*], S. Mahdavi[a], M. Rafizadeh[b]

[a]*Faculty of Chemistry, Kharazmi University, Tehran, Iran*
[b]*Faculty of Chemistry, Islamic Azad University, Shahre-Rey branch, Iran*

Received 20 October 2012; received in revised form 17 November 2012; accepted 20 November 2012
Available online 2 December 2012

Abstract

The present work reports the preparation of nickel molybdate nanocrystals via a microemulsion method. The microemulsion system included cationic surfactant CTAB, 1-butanol as co-surfactant, isooctane as oil phase, and aqueous solutions of nickel chloride and sodium molybdate. The produced water pools in the microemulsion system act as nanoreactors for reaction of nickel and molybdate ions to produce nickel molybdate nanomaterial. After calcination, the structure and morphology of the product were characterized by Fourier-transform infrared (FT-IR) and UV–vis spectroscopies, X-ray diffraction (XRD), energy-dispersive X-ray analysis (EDX), transmission electron microscopy (TEM), and thermogravimetric analyses (TGA). The synthesized α-$NiMoO_4$ nanocrystals have a monoclinic structure with lengths of 140–150 nm and widths of 60–70 nm.

Keywords: Nickel molybdate; Microemulsion; Nanocrystals; Reverse micelles

1. Introduction

Metal molybdates are of great technological interest due to their attractive properties, especially potential applications in catalysis [1–9]. Among them nickel molybdates have become more important because of their application in catalysis such as oxidative dehydrogenation of light alkanes [10,11], hydrodesulfurization, hydrodenitrogenation [12,13], etc. There are two stable structures for stoichiometric $NiMoO_4$ [14], in which the α-form is stable at room temperature and contains molybdenum in an octahedral environment. The β-form, which is stable at high temperature, has the molybdenum in a tetrahedral configuration. The α-$NiMoO_4$ has monoclinic structure and its structural units are NiO_6 and MoO_6 octahedra, which share edges and form chains.

Up to now, many investigations have been carried out on the synthesis of nickel molybdate materials [8,15–17]. The most common preparation method used for the preparation of nickel molybdate is the co-precipitation technique and the effects of various parameters on the resulting product have been investigated [8,15]. Other techniques include reactive sputtering [16], thermal treatment of organic salts [17], and sonochemical synthesis [18].

On the other hand, the development of uniform nanoparticles has been greatly pursued in recent years [18–24]. Due to their interesting electronic, optical, magnetic, and chemical properties, these nanosized materials have promising applications in many areas such as microelectronic devices, catalysis, biomedicine and so on. As a result, the preparation of uniform sized nanoparticles has become a very important research area and various techniques have been used for this purpose.

There are some reports on the preparation of nickel molybdate nanostructures such as mechanochemical synthesis [25], complete evaporation of a polymer-based metal complex precursor solution [26,27], sonochemical method [28], and hydrothermal method [29]. However, to the best of our knowledge, there is no report on the preparation of nickel molybdate nanoparticles with the microemulsion method. Recently, we reported successful preparation of bismuth and iron molybdate nanoparticles using the microemulsion method [30,31]. Nanoparticle

*Corresponding author. Tel./fax: +98 263 4551023.
E-mail address: mfarahany@yahoo.com (M. Masteri-Farahani).

0272-8842/$ - see front matter © 2012 Elsevier Ltd and Techna Group S.r.l. All rights reserved.
http://dx.doi.org/10.1016/j.ceramint.2012.11.059

preparation in microemulsions has been an interesting research topic in recent years and a large number of different nanomaterials have been synthesized in water-in-oil microemulsions [32]. The microemulsion method provides good control over the size and shape of the prepared nanomaterials and produces uniform and monodispersed nanomaterials.

Herein we report for the first time the preparation and characterization of uniform nickel molybdate nanocrystals by using the microemulsion method. The advantage of this approach is better control over the size and shape of the final nickel molybdate nanocrystals in comparison to other methods.

2. Experimental

All chemical reagents (nickel nitrate, sodium molybdate, n-butanol, isooctane, and cetyltrimethyl ammonium bromide) were purchased from the Merck chemical company.

In a typical procedure 3 ml aqueous solution of $Ni(NO_3)_2$ (0.1 M) was added to a mixture of n-butanol (2 g)/isooctane (4 g)/CTAB (2 g) in water (2 ml) and the resulting mixture was stirred for 15 min until a transparent solution was obtained. After that, 3 ml aqueous solution of Na_2MoO_4 (0.1 M) was added to the above mixture to give a final molar ratio of $[Ni^{2+}]/[MoO_4^{2-}]=1$. The resultant mixture was stirred for 12 h at room temperature. The obtained precipitate was separated by centrifugation and then washed several times with distilled water and ethanol and dried in a vacuum oven at 383 K. Finally, the resulting precipitate was calcined at 400 °C for 8 h.

X-ray diffraction (XRD) patterns of the prepared nanocrystals were recorded with a SIEFERT XRD 3003 PTS diffractometer using Cu Kα radiation ($\lambda=0.1542$ nm). FT-IR spectra were obtained with a Perkin–Elmer Spectrum RXIFT-IR spectrometer using pellets of the materials diluted with KBr. UV–vis spectra were collected with a PG Instrument Ltd. T90+ UV/vis spectrometer with $BaSO_4$ as standard. The morphology and particle size of the prepared nanocrystals were observed by using a transmission electron microscope (Philips EM 208S instrument with an accelerating voltage of 100 kV). Elemental analyses were performed by a scanning electron microscope with an EDX detector INCA Penta FETx3. Thermogravimetric measurements were made on a Perkin Elmer Diamond thermogravimeter. The temperature was increased to 700 °C using a rate of 10 °C/min in static air.

3. Result and discussion

It is well known that $NiMoO_4$ could be formed through the reaction between Ni^{2+} and MoO_4^{2-} ions [8]. We conducted the preparation of $NiMoO_4$ with the reverse micelles acting as nanoreactors. Fig. 1 shows a schematic representation of all stages involved in the synthesis of $NiMoO_4$ nanocrystals by the microemulsion method. Stoichiometric addition of the MoO_4^{2-} solution to the microemulsion containing Ni^{2+} ions gives rise to the immediate formation of $NiMoO_4$ precipitates within the reverse micelles. The CTAB species stabilize the obtained nanoparticles by capping their external surfaces. The organic shells adsorbed on the external surfaces of the product can keep the nanoparticles apart from each other by presenting a strong steric hindrance to overcome van der Waals interactions between the nanoparticles. It promotes the formation of nanoparticles with narrow size and shape distribution. Our earlier studies based on X-ray diffraction analysis have shown that the product formed in the first stage is amorphous in nature. The as-prepared $NiMoO_4$ nanoparticles were calcined at 400 °C in order to obtain the α-crystallized $NiMoO_4$ product.

The thermogravimetric analysis of the as-prepared $NiMoO_4$ nanoparticles was conducted at a heating rate of 10 °C/min between room temperature and 700 °C, and the results are shown in Fig. 2. The TGA curve indicates four different stages of mass reduction as a function of temperature. As our results show, first mass loss occurs in the region from room temperature to 177 °C which is due to the loss of adsorbed water. Due to the removal of adsorbed water the corresponding DTA curve in this region is endothermic. The second stage of mass loss takes place in the region from 177 to 280 °C and third from 280 to 430 °C which are assigned to the combustion of organic compounds and CTA^+ cations, and are in good agreement with exothermic DTA peaks in these regions. The fourth stage of mass reduction between 430 and 480 °C is probably due to phase transition to β-$NiMoO_4$ with slight loss of water produced during the dehydroxylation process. The corresponding DTA curve for this stage is exothermic. It is well known that monoclinic α-$NiMoO_4$ can be transformed to β-$NiMoO_4$ upon heat treatment. According to the TGA analysis, the prepared α-$NiMoO_4$ nanoparticles transformed to β-$NiMoO_4$ at 430–480 °C. Thus, appropriate calcination temperature for crystallization of the as-prepared material while preventing the formation of β-$NiMoO_4$ is 400 °C.

FT-IR spectroscopy was used to confirm the phases present in the prepared nanomaterials. Fig. 3 shows the FT-IR spectra of the as-prepared and calcined products. In the FT-IR spectrum of the as-prepared nanoparticles (Fig. 3a), the bands at 2854 and 2923 cm^{-1} are attributed to the asymmetrical and symmetrical C–H stretching vibrations of CH_2 groups of CTAB species associated with the as-prepared nanoparticles,respectively. Also, the bands at 1400–1500 cm^{-1} were assigned to the symmetrical and asymmetrical C–H deformations. The bands in the range of 800–900 cm^{-1} are assigned to the stretching vibrations of the Mo–O–Mo groups and the absorption bands in the range of 400–600 cm^{-1} are attributed to the superposition of stretching vibrations of MoO_6 and NiO_6 groups. In the FT-IR spectrum of the calcined product (Fig. 3b), the bands due to the presence of the C–H groups disappeared as a result of the combustion and removal of CTAB species. On the other hand, the bands at 930–970 cm^{-1} are assigned to ν_1 vibration of the distorted MoO_6

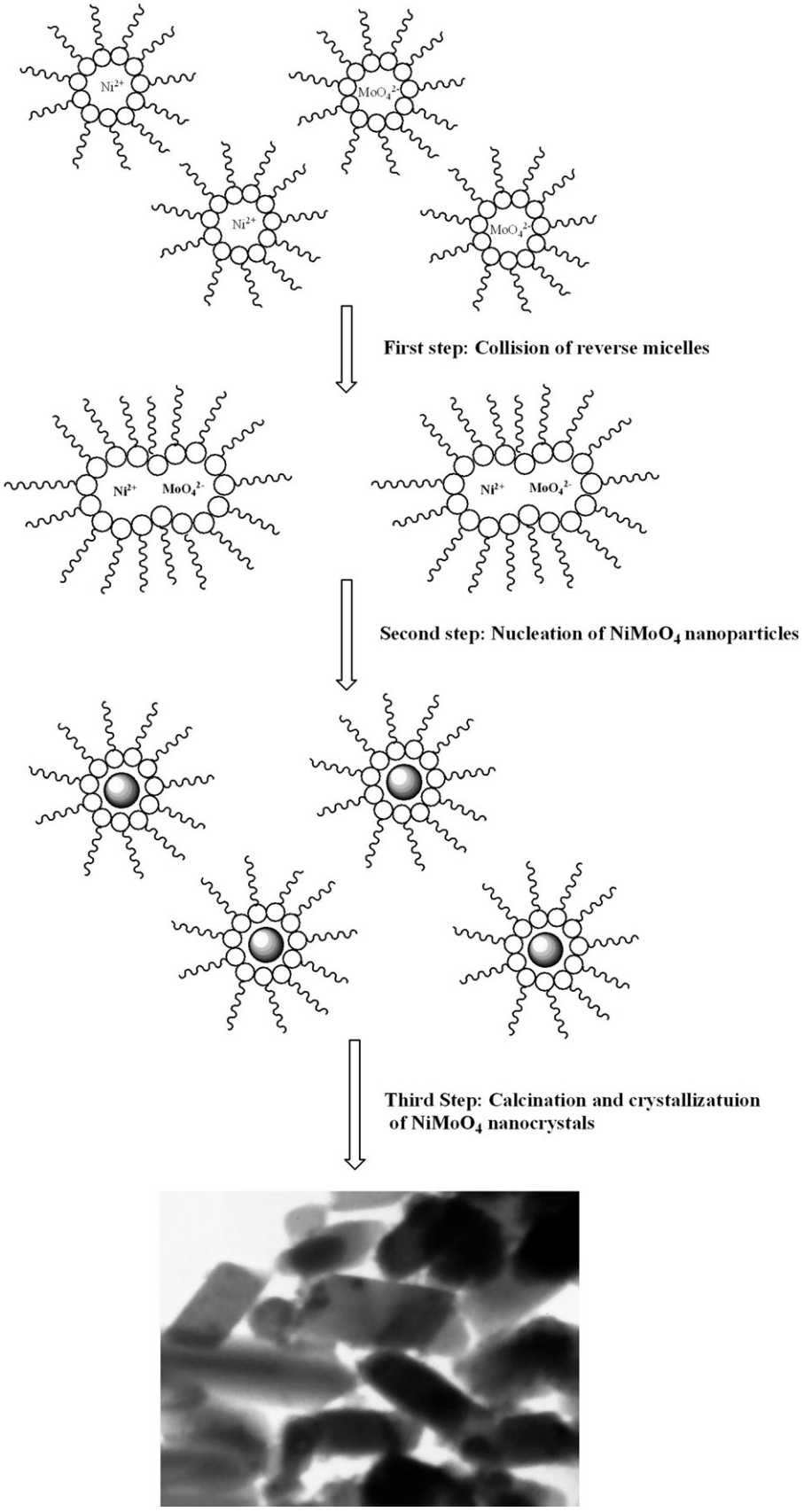

Fig. 1. Schematic representation of all stages involved in the synthesis of $NiMoO_4$ nanocrystals.

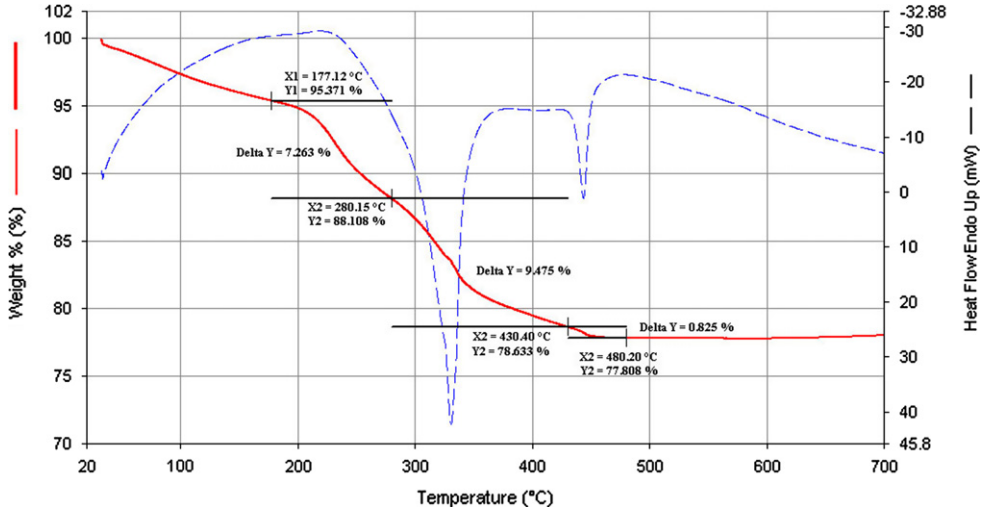

Fig. 2. TGA–DTA curves of the as-prepared $NiMoO_4$ nanoparticles.

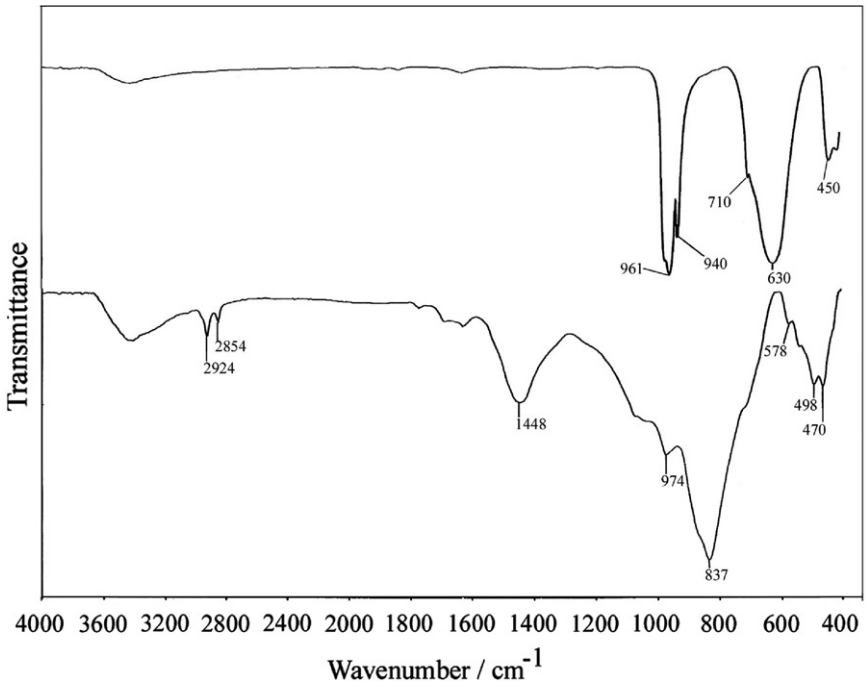

Fig. 3. FT-IR spectra of the (a) as-prepared and (b) calcined nanomaterials.

octahedra present in the crystalline α-$NiMoO_4$. The bands in the range of 600–700 cm^{-1} are attributed to ν_3 vibrations of the same units. The low energy bands at 420–450 cm^{-1} are a superposition of ν_4 and ν_5 of MoO_6 and ν_3 of NiO_6 groups in the α-$NiMoO_4$ nanocrystals [8,25].

There are no distinguished peaks of β-$NiMoO_4$ at 806 and 880 cm^{-1} in the FT-IR spectrum of the calcined product [8]. On the other hand, the lack of any peak at 980 cm^{-1} attributed to the Mo=O vibrations indicates the absence of MoO_3 material. So, it may be concluded that the product is pure α-$NiMoO_4$ nanocrystals.

The UV–vis spectrum of the prepared α-$NiMoO_4$ nanocrystals is shown in Fig. 4. The spectrum shows a strong absorption located at 267 nm wavelength associated with a shoulder near 340 nm which is mainly attributed to the LMCT charge-transfer transition (from 2p orbitals of oxygen to 4d orbitals of molybdenum) inside the MoO_4^{2-} anion [33]. The weak broad absorption located at 420–550 nm can be assigned to spin allowed d–d transitions of Ni^{2+} ion with d^8 electronic configuration.

The optical band gap of the prepared α-$NiMoO_4$ nanocrystals was evaluated from the UV–vis absorption spectrum using the Tauc equation [34]. The calculated band gap value (E_g=3.2 eV) was found to be higher than that of bulk $NiMoO_4$ (0.2 eV) [35] as a result of quantum confinement of α-$NiMoO_4$ nanocrystals.

Phase composition and structure of the calcined sample was further examined by X-ray powder diffraction analysis. XRD

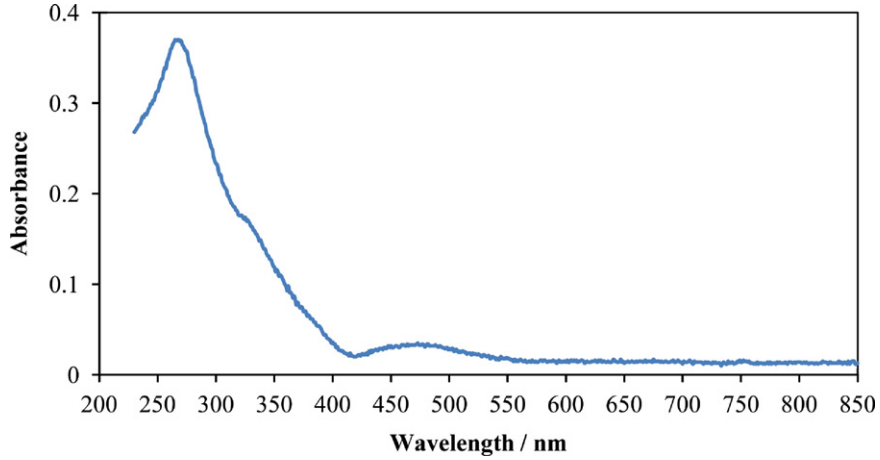

Fig. 4. UV–vis spectrum of the prepared α-$NiMoO_4$ nanocrystals.

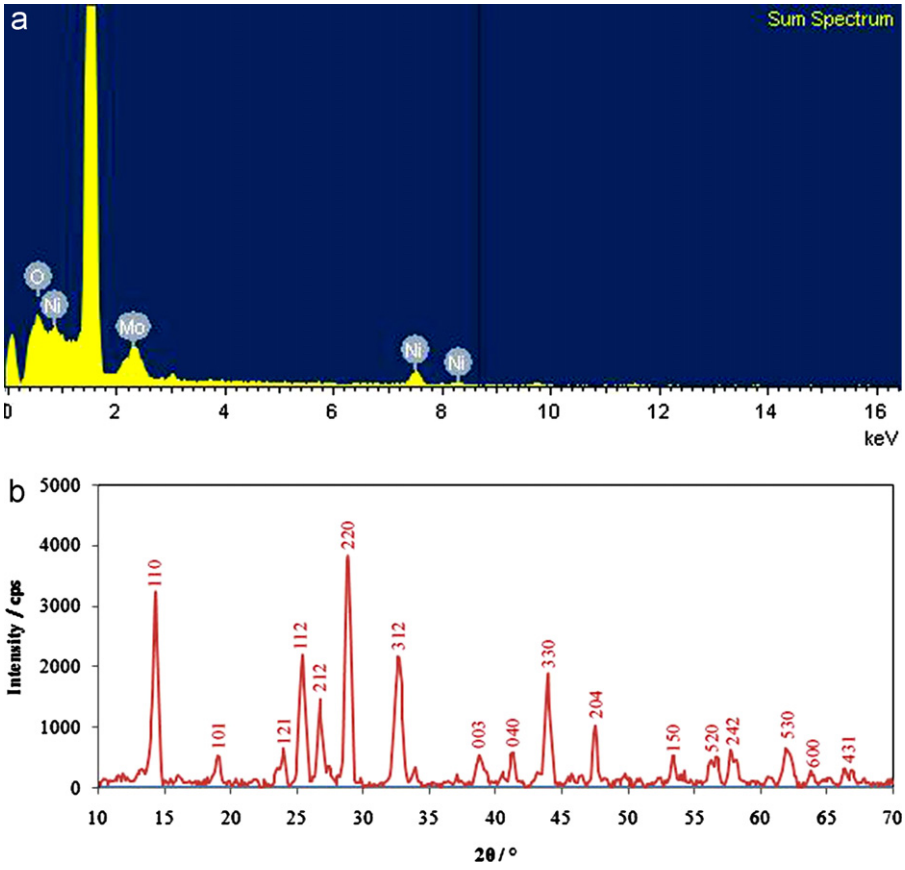

Fig. 5. (a) XRD pattern and (b) EDX analysis of the prepared nanocrystals after calcination.

pattern of the prepared nanocrystals after calcination is shown in Fig. 5a. As indicated in this figure, the pattern exhibits all peaks corresponding to monoclinic α-$NiMoO_4$ material with unit cell dimensions $a=9.509$ Å, $b=8.759$ Å, $c=7.667$ Å, and $\beta=113.13^{\circ}$, and can be indexed according to JCPDS Card No. 33-0948. The sharp diffraction peaks are an indication of the long range order and good crystallinity of the prepared nanomaterial and the absence of characteristic peaks of other impurities such as β-$NiMoO_4$ or MoO_3 phases indicates the high purity of the product.

Stoichiometry and chemical composition of the prepared nanomaterial were examined by energy-dispersive X-ray analysis (EDX). EDX analysis of the nickel molybdate nanocrystals in Fig. 5b shows the molar ratio Ni:Mo of 1:1.1 which is near the stoichiometric composition and further confirms the formation of α-$NiMoO_4$ nanocrystals.

The morphology and microstructure of the calcined product were investigated by transmission electron microscopy (TEM), and a typical TEM image is shown in Fig. 6.

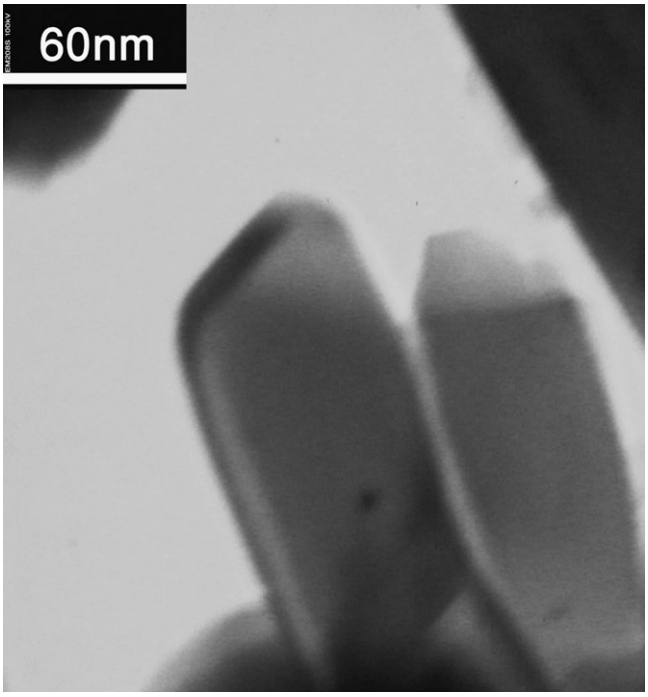

Fig. 6. TEM image of the prepared α-$NiMoO_4$ nanocrystals.

The TEM image clearly shows that the prepared nanocrystals have monoclinic structure with lengths of 140–150 nm and widths of 60–70 nm.

4. Conclusion

Monodispersed α-$NiMoO_4$ nanocrystals were synthesized by using a microemulsion system including cationic surfactant CTAB/1-butanol/isooctane and water. Our studies suggested that 400 °C temperature is adequate to obtain high quality α-$NiMoO_4$ nanocrystals with good crystallinity and perfect morphology. The XRD results show the presence of pure monoclinic α-$NiMoO_4$ nanocrystals and from EDX analysis the atomic ratio of Ni to Mo was shown to be 1:1.1. The TEM analysis shows that the α-$NiMoO_4$ nanocrystals have monoclinic crystal geometry. The main advantage of the presented method is the preparation of monodispersed pure phase α-$NiMoO_4$ nanocrystals.

References

[1] N.I. Inescu, M. Caldararu, Heterogeneous Selective Oxidation of Lower Olefins, Editura Academiei Romane, Bucharest, 1993, p. 278.
[2] R.K. Grasselli, Fundamental principles of selective heterogeneous oxidation catalysis, Topics in Catalysis 21 (2002) 79–88.
[3] A.M. Beale, G. Sankar, In situ study of the formation of crystalline bismuth molybdate materials under hydrothermal conditions, Chemistry of Materials 15 (2003) 146–153.
[4] H.H. Li, K.W. Li, H. Wang, Hydrothermal synthesis and photocatalytic properties of bismuth molybdate materials, Materials Chemistry and Physics 116 (2009) 134–139.
[5] A.P.V. Soarez, M.F. Portela, Methanol selective oxidation to formaldehyde over iron-molybdate catalysts, Catalysis Reviews 47 (2004) 125–174.
[6] A.P.V. Soarez, M.F. Portela, A. Kiennemann, L. Hilaire, J.M.M. Millet, Iron molybdate catalysts form ethanol to formaldehyde oxidation: effects of Mo excess on catalytic behavior, Applied Catalysis A 206 (2001) 221–229.
[7] A.M. Beale, S.D.M. Jacques, E.S. Parvalescu, M.G. O'Brian, P. Barnes, B.M. Weckhuysen, An iron molybdate catalyst for ethanol to formaldehyde conversion prepared by a hydrothermal method and its characterization, Applied Catalysis A 363 (2009) 143–152.
[8] L.M. Madeira, M.F. Portela, C. Mazzocchia, Nickel molybdate catalysts and their use in the selective oxidation of hydrocarbons, Catalysis Reviews 46 (2004) 53–110.
[9] B. Pillay, M.R. Mathebula, H.B. Friedrich, Applied Catalysis A 361 (2009) 57–64.
[10] A. Kaddouri, R. Anouchinsky, C. Mazzocchia, L.M. Madeira, M.F. Portela, Oxidative dehydrogenation of ethane on the α and β phases of $NiMoO_4$, Catalysis Today 40 (1998) 201–206.
[11] B. Pillay, M.R. Mathebula, H.B. Friedrich, The oxidative dehydrogenation of n-hexane over Ni–Mo–O catalysts, Applied Catalysis A 361 (2009) 57–64.
[12] R.A. Madeley, S. Wanke, Applied Catalysis 39 (1988) 295–314.
[13] B.C. Gates, J.R. Katzer, G.C.A. Schuit, Chemistry of Catalytic Processes, McGraw-Hill, New York, 1979, p. 390.
[14] A.W. Sleight, B.L. Chamberland, Inorganic Chemistry 7 (1968) 1672.
[15] R.N. Singh, M.R. Awasthi, A.S.K. Sinha, Preparation and electrochemical characterization of a new $NiMoO_4$ catalyst for electrochemical O_2 evolution, Journal of Solid State Electrochemistry 13 (2009) 1613–1619.
[16] J.Y. Zou, G.L. Schrader, Multicomponent thin film molybdate catalysts for the selective oxidation of 1,3-butadiene, Journal of Catalysis 161 (1996) 667–686.
[17] C. Mazzocchia, A. Kaddouri, R. Anouchinsky, M. Sautel, G. Thomas, On the NiO–MoO_3 mixed oxide correlation between preparative procedures thermal activation and catalytic properties, Solid State Ionics 63–65 (1993) 731–735.
[18] G. Schmid, Clusters and Colloids: From Theory to Application, VCH, NewYork, 1994.
[19] J.H. Fendler, Nanoparticles and Nanostructured Films, Wiley–VCH, Weinheim, 1998.
[20] G. Schmid, Large clusters and colloids—metals in the embryonic state, Chemical Reviews 92 (1992) 1709–1727.
[21] K. Holmberg, Surfactant-templated nanomaterials synthesis, Journal of Colloid and Interface Science 274 (2004) 355–364.
[22] A. Henglein, Small-particle research—physicochemical properties of extremely small colloidal metal and semiconducting particles, Chemical Reviews 89 (1989) 1861–1873.
[23] J. Belloni, Metal nanocolloids, Current Opinion in Colloid and Interface Science (1996) 184–196.
[24] T.S. Ahmadi, Z.L. Wang, T.C. Green, A. Henglein, M.A. El-Sayed, Shape controlled synthesis of colloidal platinum nanoparticles, Science 272 (1996) 1924–1926.
[25] D. Klissurski, M. Mancheva, R. Iordanova, G. Tyuliev, B. Kunev, Mechanochemical synthesis of nanocrystalline nickel molybdates, Journal of Alloys and Compounds 422 (2006) 53–57.
[26] A. Sen, P. Pramanik, Low-temperature synthesis of nano-sized metal molybdate powders, Materials Letters 50 (2001) 287–294.
[27] A. Sen, P. Pramanik, A chemical synthetic route for the preparation of fine-grained metal molybdate powders, Materials Letters 52 (2002) 142–146.
[28] G. Kianpour, M. Salavati-Niasari, H. Emadi, Sonochemical synthesis and characterization of $NiMoO_4$ nanorods, Ultrasonic, Sonochemistry 20 (2013) 418–424.
[29] Y. Ding, Y. Wan, Y.L. Min, W. Zhang, S.H. Yu, General synthesis and phase control of metal molybdate hydrates $MMoO_4$ nH_2O (M=Co, Ni, Mn, and n=0, 3/4, 1) nano/microcrystals by a hydrothermal approach: magnetic, photocatalytic, and electrochemical properties, Inorganic Chemistry 47 (2008) 7813–7823.

[30] M. Masteri-Farahani, H.S. Hosseini, Synthesis and characterization of bismuth molybdate nanoparticles within nanoreactors of reverse micelles, Powder Technology 228 (2012) 228–230.
[31] M. Masteri-Farahani, M. Sadrinia, Synthesis and characterization of ferric molybdate nanoparticles in reverse micelles nanoreactors, Powder Technology 217 (2012) 554–557.
[32] L.B. Cushing, V.L. Kolesnichenko, C.J. O'Connor, Recent advances in the liquid-phase synthesis of inorganic nanoparticles, Chemical Reviews 104 (2004) 3893–3946.
[33] K. Nakamoto, Infrared and Raman Spectra of Inorganic and Coordination Compounds, fourth edition, John Wiley and Sons, Inc., New York, 1986.
[34] J. Tauc, R. Grigorovici, A. Vancu, Optical properties and electronic structure of amorphous germanium, Physica Status Solidi 15 (1966) 627–637.
[35] S.F. Matar, A. Largeteau, G. Demazeau, $AMoO_4$ (A=Mg, Ni) molybdates: phase stabilities, electronic structures and chemical bonding properties from first principles, Solid State Sciences 12 (2010) 1779–1785.